

Surface-enhanced fluorescence and application study based on Ag-wheat leaves

Hongwen Cao(曹红文), Liting Guo(郭立婷), Zhen Sun(孙祯), Tifeng Jiao(焦体峰), and Mingli Wang(王明利)
Citation: Chin. Phys. B, 2022, 31 (**3**): 037803. DOI: 10.1088/1674-1056/ac1f0d
Journal homepage: http://cpb.iphy.ac.cn; http://iopscience.iop.org/cpb
What follows is a list of articles you may be interested in

Magnetic polaron-related optical properties in Ni(II)-doped CdS nanobelts: Implication for spin nanophotonic devices

Fu-Jian Ge(葛付建), Hui Peng(彭辉), Ye Tian(田野), Xiao-Yue Fan(范晓跃), Shuai Zhang(张帅), Xian-Xin Wu(吴宪欣), Xin-Feng Liu(刘新风), and Bing-Suo Zou(邹炳锁)
Chin. Phys. B, 2022, 31 (**1**): 017802. DOI: 10.1088/1674-1056/ac0782

Polarized photoluminescence spectroscopy in WS_2, WSe_2 atomic layers and heterostructures by cylindrical vector beams

Lijun Wu(吴莉君), Cuihuan Ge(葛翠环), Kai Braun, Mai He(贺迈), Siman Liu(刘思嫚), Qingjun Tong(童庆军), Xiao Wang(王笑), and Anlian Pan(潘安练)
Chin. Phys. B, 2021, 30 (**8**): 087802. DOI: 10.1088/1674-1056/abf3b6

Linear and nonlinear optical response of g-C_3N_4-based quantum dots

Jing-Zhi Zhang(张竞之) and Hong Zhang(张红)
Chin. Phys. B, 2021, 30 (**7**): 077802. DOI: 10.1088/1674-1056/abec2f

Low-dimensional phases engineering for improving the emission efficiency and stability of quasi-2D perovskite films

Yue Wang(王月), Zhuang-Zhuang Ma(马壮壮), Ying Li(李营), Fei Zhang(张飞), Xu Chen(陈旭), and Zhi-Feng Shi(史志锋)
Chin. Phys. B, 2021, 30 (**6**): 067802. DOI: 10.1088/1674-1056/abe92b

Localized electric-field-enhanced low-light detection by a 2D SnS visible-light photodetector

Hao Wen(文豪), Li Xiong(熊力), Congbing Tan(谭丛兵), Kaimin Zhu(朱凯民), Yong Tang(唐勇), Jinbin Wang(王金斌), and Xiangli Zhong(钟向丽)
Chin. Phys. B, 2021, 30 (**5**): 057803. DOI: 10.1088/1674-1056/abd7db

---

Surface-enhanced fluorescence and application study based on Ag-wheat leaves

Hongwen Cao(曹红文)[1], Liting Guo(郭立婷)[1], Zhen Sun(孙祯)[1], Tifeng Jiao(焦体峰)[2,†], and Mingli Wang(王明利)[1,‡]

[1] *State Key Laboratory of Materials Science & Technology and Key Laboratory for Microstructural Material Physics of Hebei Province, School of Science, Yanshan University, Qinhuangdao* 066004, *China*

[2] *Hebei Key Laboratory of Applied Chemistry, School of Environmental and Chemical Engineering, Yanshan University, Qinhuangdao* 066004, *China*

(Received 14 June 2021; revised manuscript received 1 August 2021; accepted manuscript online 19 August 2021)

Wheat leaves with natural microstructures as substrates were covered by the silver nanoislands by magnetron to prepare a low-cost, environment-friendly and mass production surface-enhanced fluorescence (SEF) substrate (Ag-WL substrate). The best SEF substrate was selected by repeatly certifying the fluorescence intensity of 10^{-5} M Rhodamine B (RB) and 10^{-5} M Rhodamine 6G (R6G) aqueous solutions. The abundant semi-spherical protrusions and flake-like structures on the surface of the Ag-WL substrate produce high-density hot spots, which provides a new and simple idea for the preparation of biomimetic materials. The results of 3D finite-different time-domain (FDTD) simulation show that the nanoisland gap of semi-spherical protrusions and flake-like structures has produced rich hotspots. By adjusting the time of magnetron sputtering, the enhancement factor (EF) was as high as 839 times, relative standard deviation (RSD) reached as low as 10.7%, and the substrate was very stable and repeatable, which shows that Ag-WL substrate is trustworthy. Moreover, semi-spherical protrusions provide stronger surface-enhanced Raman scattering (SERS) effects compared to flake-like structure. What is more surprising is that the detection limit of the substrate for toxic substance crystal violet (CV) is as low as 10^{-10} M.

Keywords: surface-enhanced fluorescence, wheat leaf, crystal violet, semi-spherical protrusions

PACS: 78.67.–n, 78.55.–m, 73.20.–r **DOI:** 10.1088/1674-1056/ac1f0d

1. Introduction

In the view of characteristics of good selectivity and high sensitivity, fluorescence detection technology has been widely used in the fields of environmental science, biosensing and so on.[1–4] Along with more and more detailed exploration of the micro world, it is imperative to improve the sensitivity of fluorescence detection. Therefore, surface-enhanced fluorescence (SEF) technology has become a research hotspot in recent years. Generally speaking, SEF phenomenon originates from the surface plasmon resonance behavior of metal nanoparticles, which is closely related to the size and morphology of metal nanoparticles. The noble metal nanoparticles assembly for SEF include plate,[5,6] microspheres,[7,8] and hydrosol system.[9,10]

In general, the preparation of SEF substrates frequently pay more attention to colloidal structures such as nanoparticles[11] and core-shell structure.[12,13] However, above substrate are difficult to be repeatly prepared due to the low stability and complex synthesis steps.[14] Therefore, we have discovered a more simple and easy method to produce diverse morphology substrate. It can be found that high performance SEF substrates were obtained by controlling the growth conditions of silver nanoislands. The metal silver has the characteristics of sharp LSPR resonance band and high refractive index sensitivity, which is more favorable to produce LSPR effect.[15–17] Moreover, as a natural biomaterial, wheat leaves not only show the advantages of low price and environmental protection, but also have unique semi-spherical protuberant and flake-like nanostructures, which provide abundant surface area for the generation of hot spots. The complex morphologies of metal nanostructures with more "hot spots" can produce higher fluorescence enhancement. In the process of molecular detection, different detection substances often need to use different detection means. In order to achieve a better enhancement effect, it is necessary to design different morphology of surface reinforcement substrate. What's more, the biological SEF substrate can effectively avoid the aggregation phenomenon caused by traditional chemical deposition and the high cost in large-scale production.[18] Compared with etching technology, magnetron sputtering has more significant merits, namely, less damage, easy large-scale preparation and low cost.[19–21]

In this paper, magnetron sputtering method was used to prepare SEF substrates with high density hot spots. Figure 1 briefly illustrates the process of preparing substrates and detecting fluorescence on wheat leaves. Firstly, silver nanoislands were deposited on wheat leaves. A series of Ag-WL SEF

†Corresponding author. E-mail: tfjiao@ysu.edu.cn
‡Corresponding author. E-mail: wml@ysu.edu.cn

© 2022 Chinese Physical Society and IOP Publishing Ltd

substrates with different micro-morphology were obtained by controlling the magnetron sputtering time. And then, the substrate with the optimum SEF effect was selected according to the change of emission intensities of R6G and RB solution. The enhancement factor of Ag-WL SEF substrates reached as high as 961 times with fine stability and reproducibility. Furthermore, SERS spectroscopy was used to analyze the surface enhancement of different structures of the substrate. At the same time, we also calculated the electromagnetic field distribution of the Ag-WL-40 substrate by 3D-FDTD method, showing the distribution of hot spots distribution. Finally, the Ag-WL SEF substrate was used for the detection of toxic substance CV, whose detection limit reached $\sim 10^{-10}$ M.

2. Experiment

2.1. Materials and instruments

All the wheat leaves were purchased from Shengliyuan flower shop (Shanghai, China). Ag target (99.99%) material was purchased from Nanchang Material Technology Co., Ltd. Probe molecules Rhodamine B (RB, $C_{28}H_{31}ClN_2O_3$) and Rhodamine 6G (R6G, $C_{28}H_{31}N_2O_3Cl$) were obtained from J&K Scientific LTD (Beijing, China). The absolute alcohol was procured from Aladdin-holdings group (Beijing, China). Crystal violet (CV, $C_{25}H_{30}ClN_3$) was bought from Tianjin Kemiou Chemical Reagent Co., Ltd. (Tianjin, China). The Ultra-pure water used in the experiment was prepared in the Key Laboratory for Microstructural Material Physics of Hebei Province. Besides, wheat leaves were modified by silver nanoparticles with direct-current (DC) magnetron sputtering apparatus (JGP450). The microstructure and phase structure of Ag-WL substrate were analyzed by scanning electron microscope (SEM, Hitachi S-4800II) and x-ray diffraction (XRD, D/Max-2500/PC). The fluorescence spectra were acquired by fluorescence spectrometer (F-7000). The ultraviolet–visible (UV–Vis) absorption spectra of the solution and the substrate were obtained by the ultraviolet spectrophotometer (UV-2550). Raman spectra of Ag-WL substrate were analyzed by inVia Raman system.

2.2. Preparation and characterization of substrates

All the wheat leaves were washed by ultrasonic for 5 min and added into anhydrous ethanol to remove dust, then dried naturally. A series of 1 cm×2 cm wheat leaves as substrates were prepared by magnetron sputtering apparatus at about 440 V, 300 mA and 2 Pa argon pressure. Subsequently, the morphology of the substrate was controlled by adjusting the magnetron sputtering time. According to different preparation time (15 min, 20 min, 25 min, 30 min, 35 min, 40 min and 45 min), the samples was named correspondingly as Ag-WL-*X* (Ag-WL-15, Ag-WL-20, Ag-WL-25, Ag-WL-30, Ag-WL-35 Ag-WL-40 and Ag-WL-45). All prepared substrates were stored in sample bags to reduce the impact of metal oxidation on the experiment.

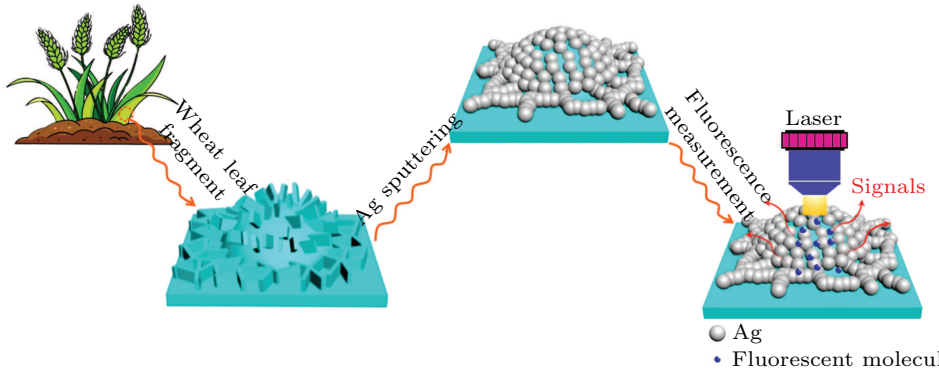


Fig. 1. Schematic illustration of the processes for preparing substrate on wheat leaves decorated with Ag by magnetron sputtering and the spectra measurement of Ag-WL substrate.

2.3. Measurements of SEF and SERS spectra

Firstly, RB solution with concentration of 10^{-2} M and 10^{-5} M was obtained by continuously dilution with ultra-pure water. R6G solution with the concentration of 10^{-5} M and the CV aqueous solution with the concentration of 10^{-10}–10^{-4} M were prepared by the same method. The experimental diagram and schematic diagram of sandwich structure used in fluorescence spectrum measurement are shown in Fig. 2, respectively. The sandwich structure is formed as follows: (a) fix the substrate on the glass sheet; (b) drip the quantitative reagent onto the substrate by pipette; (c) form water droplets on the substrate; (d) align the circular groove of the silicon glass sheet with the solution and cover it; and (e) obtain the sandwich structure of silica glass, fluorescent reagent and substrate. After, RB aqueous solution with concentration of 10^{-5} M was used as the probe molecule to select the best substrate. The experimental results were verified by using R6G solution with concentration of 10^{-5} M. Then, a certain concentration of CV solution was dropped on the optimal substrate surface, which was used to detect the practicability of the substrate. In order to reduce experimental errors, all fluorescent signals were col-

lected at room temperature during the experiment, and each solution was excited by the same laser.

In the process of SERS spectrum collection, R6G probe molecules were deposited on the substrate surface through the following methods: Firstly, 10^{-8} M R6G solution was dropped onto the Ag-WL substrate. After natural evaporation of the R6G solution on the substrate, the substrate was washed with anhydrous ethanol to remove the unbound R6G molecules. Then, above substrate was dried in nitrogen to ensure the formation of a complete R6G molecular layer on the surface of the substrate. All SERS spectra were recorded with 532 nm laser as excitation source. The incident power was 0.05 mW and the recording time was 10 s. All spectra were got from the average of 5 sets.

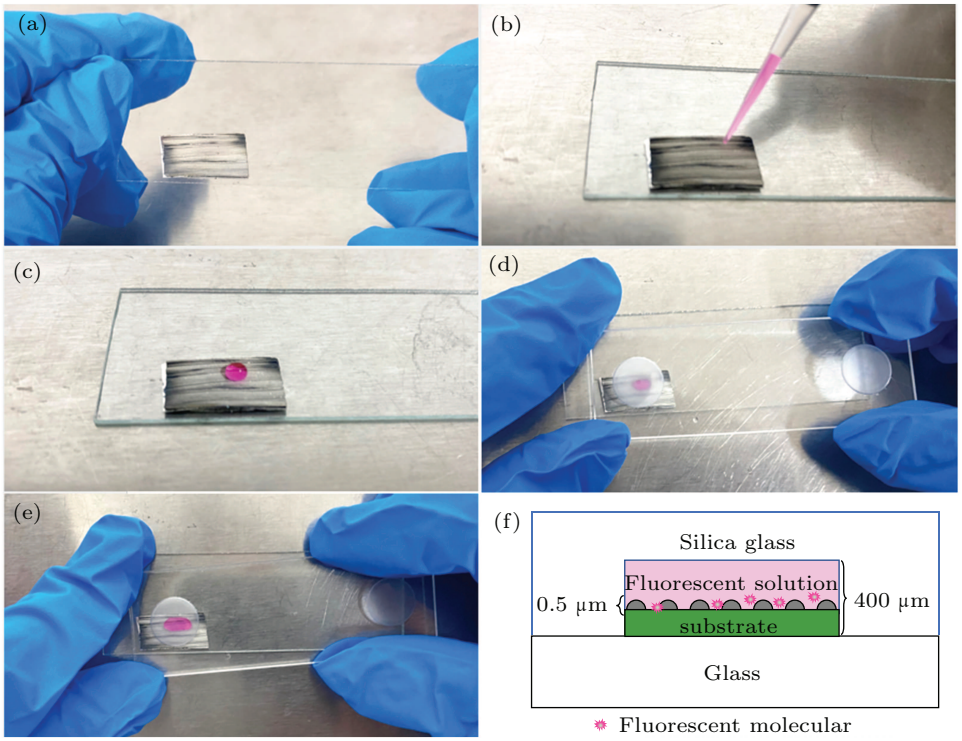


Fig. 2. (a)–(e) Photographs of the sample preparation process. (f) Schematic diagram of sandwich structure for the fluorescence measurement.

3. Result and discussion

3.1. Characteristics of substrate

Wheat is a kind of cereal crop which is widely cultivated all over the world. It not only has edible value, but also displays excellent hydrophobicity on the surface. The semi-spherical protrusions on the surface could play an indispensable role in the excellent hydrophobicity of wheat leaves. As shown in Fig. 3(a), the surface structure of wheat leaves is flake-like structure at the bottom and semi-spherical at the protruding part. The length of lamellar structure is 0.35 ± 0.1 μm. The diameter of semi-spherical protrusions is 2.9 ± 0.3 μm, and the distance between the protrusions is about 3.5 ± 0.1 μm. Through observing Fig. 3(b), the average height of semi-spherical structure of wheat leaves is measured to be approximately 2 μm. The semi-spherical protrusions are distributed irregularly, so wheat leaves may not be as noticeable as the regular nanocolumn structures of lotus leaves and cicada wings.[22] In the experiment, it is found that the modification of silver nanoparticles on wheat leaves by magnetron sputtering has a certain effect on the microstructure of wheat leaves, but it achieves good fluorescence enhancement effect. At the same time, it also provides a new method for the preparation of biomimetic materials with similar structure to wheat leaves, because there is no high requirement for the preparation process. This can be examined by the SEM images of Ag-WL-25 and Ag-WL-40, respectively, in Figs. 3(c) and 3(d). It can be seen that the microstructure of the substrate gradually changes significantly with the increase of magnetron sputtering time. The protrusions of the semi-spherical gradually becomes larger, and the silver nanoislands at the top also gradually gather and increase. By measuring the size of the semi-spherical structure and the top nanoisland in the Figs. 3(c) and 3(d), it is found that the semi-spherical structure size is 2 ± 0.5 μm and 2.5 ± 0.6 μm, respectively. The size of the nanoisland is about 50 ± 10 nm. With increasing magnetron sputtering time, the size of spheroidal structure increases gradually, and the gap between adjacent semi-spherical structures decreases gradually. Figures 3(e) and 3(f) show the enlarged SEM images of wheat leaves and Ag-WL-40. It is easy to see that the silver nanoparticles gather at the top and the density increases gradually. The top and bottom position of nanoscale Ag-WL substrate produce high den-

sity hot spots with the strong local field enhancement effect. Therefore, it is further proved that there are high density hot spots in Ag-WL substrate.

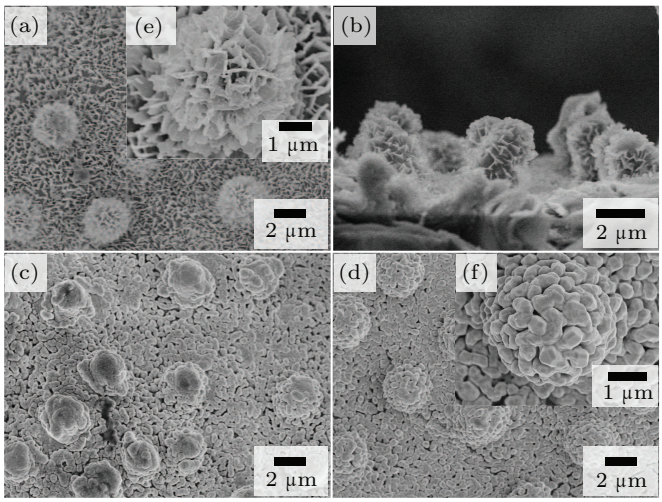


Fig. 3. Top-view SEM images of the substrate (a) wheat leaves without any decoration, (c) Ag-WL-25, (d) Ag-WL-40. (b) Side-view SEM image of wheat leaves. (e) and (f) The locally enlarged SEM images of wheat leaves and Ag-WL-40 substrate.

In addition, the composition and phase purity of the Ag-WL-40 substrate are identified by XRD. The XRD pattern with the standard card (JCPDS No. 04-0783) is displayed in Fig. 5(a). We can observe that the values of 2θ are 38.11°, 44.33°, 64.38° and 77.48°. All diffraction peaks are well coincident with these of standard card and no other impurity peak. The four diffraction peaks correspond to (111), (200), (220) and (311) planes of silver crystal respectively, and the crystallinity is good. The results show that silver is successfully modified on wheat leaves in the process of substrate preparation, and no other impurities are introduced.

3.2. SERS performance

The semi-spherical protrusions and the bottom flake-like structure on the Ag-WL substrate provide us with a new thinking. Since both SEF and surface-enhanced Raman scattering (SERS) are members of the surface-enhanced spectroscopy family, the theory associated with both of them can be traced back to Maxwell equation and Mie light scattering theory. In the Ag-WL-40 substrate, the absorption spectrum of the substrate overlaps that of the fluorescence molecular, and it can be seen that the metal nanostructure materials of substrate have the strong surface plasmon resonance (SPR) properties. The optical field energy can be localized to the surface of metallic structures, so that the surrounding electric field strength is enhanced, which can significantly improve the spectral signal intensity of their surrounding optical species. Under the excitation of light, the metal on the substrate surface will produce collective oscillation, and the electrons are localized on the metal surface. When the oscillation frequency of the local surface plasma is as the same as the excited light, LSPR is generated. SEF and SERS are closely related to the LSPR effect. So, we detected the SERS signals of the semi-spherical protrusions and the bottom flake-like structure, as shown in Fig. 4(a). And the comparison of their Raman intensities at 613 cm^{-1}, 772 cm^{-1}, 1363 cm^{-1}, 1510 cm^{-1} and 1651 cm^{-1} were shown in Fig. 4(b). It can be seen that the peak intensity of semi-spherical structure is higher than that of the flake-like structure. Compared with the flake-like structure, there are more hot spots on the semi-spherical protrusion structure, which may produce stronger SEF effect. Therefore, wheat leaves are used as the SEF substrate.

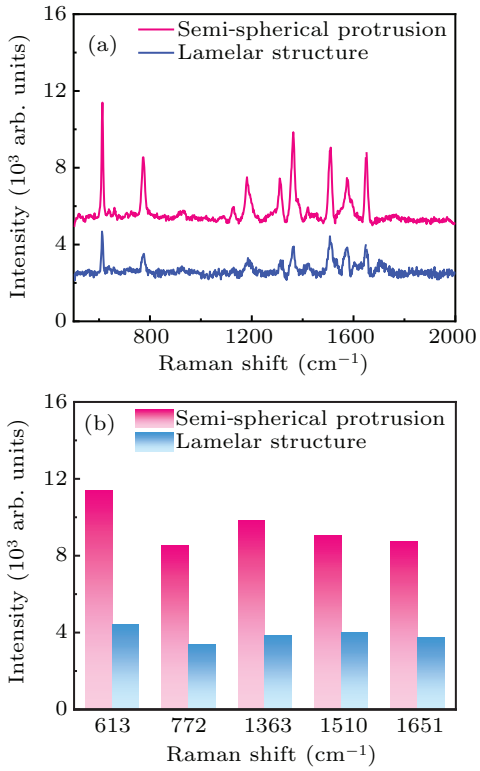


Fig. 4. (a) SERS spectra acquired by adsorption of 10^{-8} M R6G on different structures of the same substrate. (b) Comparison of SERS signal intensity at 613 cm^{-1}, 772 cm^{-1}, 1363 cm^{-1}, 1510 cm^{-1} and 1651 cm^{-1} in (a).

3.3. SEF analysis and EF calculation

RB and R6G are both common non-toxic fluorescent dyes that are easily soluble in water. In contrast, the aqueous solution of RB is bright pink color and the aqueous solution of R6G is rose-red. Because of their good photostability and high quantum yield,[23] 10^{-5} M RB and 10^{-5} M R6G aqueous solutions were selected as reagents to verify the best SEF substrates. According to different electronic energy level structure of the molecule, the excitation band of fluorescence is different. The shape and intensity of fluorescence spectrum may change under different excitation light. Before fluorescence detection, the UV-vis absorption spectra of the substrates and fluorescent reagents were obtained to find out the most suitable laser wavelength. As shown in Fig. 5(b), the absorption peaks of Ag-WL-40 substrate are in the range from UV to visible region.

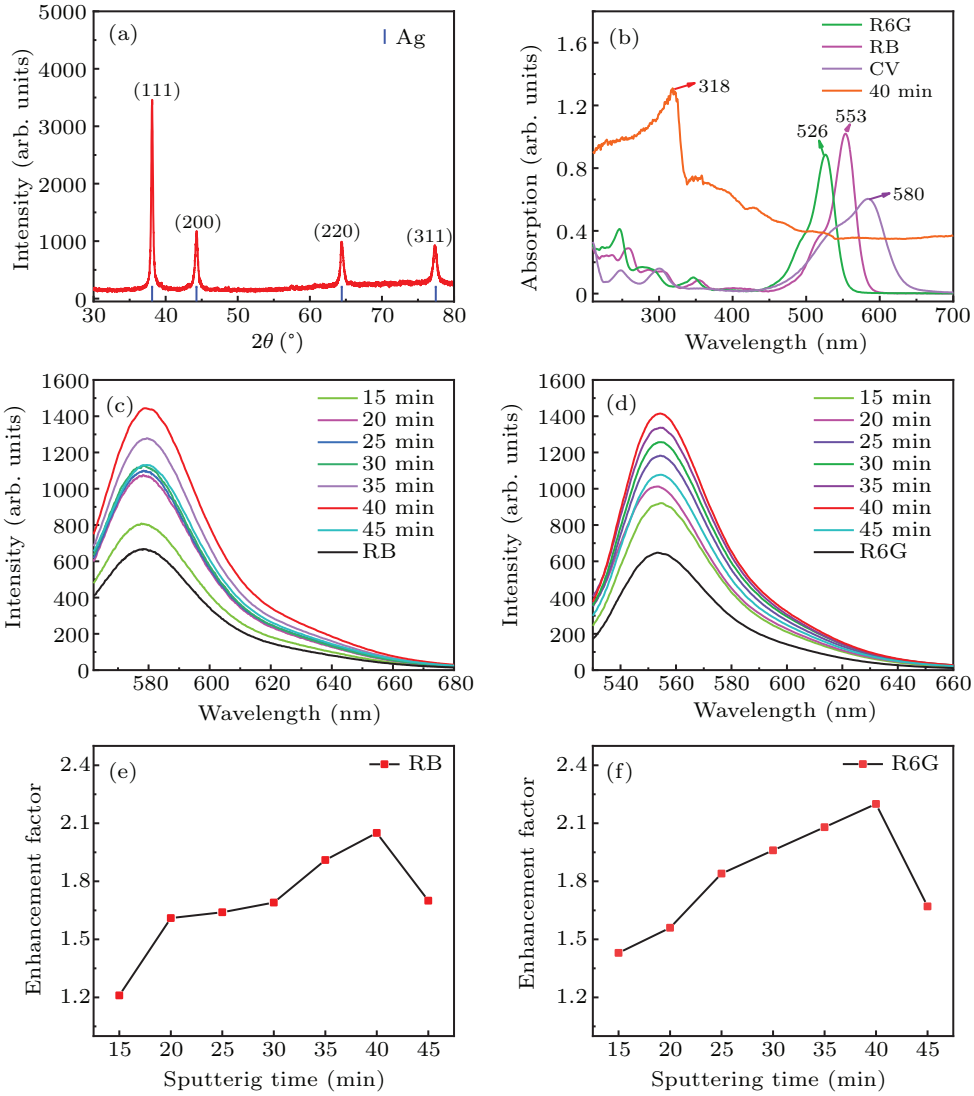


Fig. 5. (a) XRD pattern of Ag-WL-40 substrate. (b) UV–Vis absorption spectra of R6G (10^{-5} M), RB (10^{-5} M), CV (10^{-5} M), Ag-WL-40. (c), (d) The fluorescence spectra of 10^{-5} M R6G solution in the Ag-*X* substrates. (e) Change of EF at 579 nm of 10^{-5} M RB on corresponding Ag-WL substrates. (f) Change of EF at 555 nm of 10^{-5} M R6G on corresponding Ag-WL substrates.

Correspondingly, the absorption peak center of R6G (10^{-5} M), RB (10^{-5} M) and CV (10^{-5} M) appeared at 526 nm, 555 nm and 580 nm, respectively. It is known that the frequency of exciting light is consistent with the reciprocating frequency of free electrons, and the collective oscillation of Ag surface electrons will greatly increase and result in the LSPR effect, which is benefit to the fluorescence enhancement. So, it can be used as the basis for selecting excitation wavelength in the fluorescence measurement experiments. The fluorescence signal intensities of 10^{-5} M RB were obtained from the SEF Ag-WL substrates with different Ag sputtering times as also shown in Fig. 5(c) excited at 540 nm. Among the six spectral lines, the peak intensity of Ag-WL-40 spectrum line is the strongest, followed by Ag-WL-35 and Ag-WL-45 spectrum lines, and the peak intensity of Ag-WL-15 spectrum line is the weakest. The fluorescence spectrum also shows that the peak position of RB aqueous solution is at 579 nm, which indicates that the substrate has no effect on the energy level of fluorescent molecules, but improves the fluorescence intensity of molecules. This rule is also verified repeatedly by 10^{-5} M R6G aqueous solution, which also shows a similar pattern. Under excitation of 525 nm, the fluorescence spectrum measurement results are shown in Fig. 5(d). With the increase of magnetron time, the fluorescence intensity firstly increased and then decreased. The fluorescence enhancement effect was the best in Ag-WL-40 substrate. The result of this experiment is identical with Mie's theory, according to the following formula:[24]

$$C_{\text{ext}} = C_{\text{sca}} + C_{\text{abs}}, \tag{1}$$

$$C_{\text{sca}} = \frac{8\pi}{3} k^4 a^6 |\alpha|^2, \tag{2}$$

$$C_{\text{abs}} = 4\pi k a^3 \text{Im}(\alpha), \tag{3}$$

where C_{ext}, C_{sca}, and C_{abs} are represented as extinction cross section, scattering cross section and absorption cross section, respectively. α is the polarizability of a spherical particle with $r = a$, and the wave vector of the incident light is k. As the deposition time of wheat leaves increased, the size

of silver nanoisland increased gradually. According to formulas (1)–(3), under a certain excitation light, $C_{abs} \propto a^3$ and $C_{sca} \propto a^6$. Thus, C_{sca} and C_{abs} vary with the deposition time of wheat leaves. According to Mie's scattering theory, it has been known that C_{abs} and C_{sca} lead to the fluorescence quenching and fluorescence enhancement,[25] respectively. Therefore, with the increase time, the size of the silver nanoisland increases and the C_{sca} becomes larger and larger, which eventually leads to the increase of fluorescence intensity. When the excited light interacts with the silver nanoparticles, LSPR has occurred. On the one side, the surface local field generated by the nanometal structure of the substrate boosts the absorption of excited light, thus improving the absorption efficiency of the fluorescent molecules. On the other side, the enhancement of radiation resonance raises the excitation efficiency of fluorescent molecules. However, fewer and fewer fluorescent molecules can enter the cracks in the nanostructure, so the SEF effect decreases after 40 min.

In order to quantitatively estimate the fluorescence enhancement effect of Ag-WL substrate, EF was calculated by the following equation:[26]

$$\mathrm{EF} = \frac{I_{\mathrm{Ag-substrate}}}{I_{\mathrm{reference}}}, \tag{4}$$

where $I_{\mathrm{Ag-substrate}}$ and $I_{\mathrm{reference}}$ represent the fluorescence intensity values measured Ag-WL substrate and silicon glass, respectively. The relationship between EF and magnetron sputtering time is shown in Figs. 5(e) and 5(f). The groove depth of customized silica glass is 400 μm. The SEF effect can only be generated within the limits of 20 nm from the silver nanoparticles,[27] and most of the fluorescent molecules do not produce SEF effect. Thus, it is necessary to revise EF. The enhancement effect in the range of 500 nm from the substrate has great research value, as shown in Fig. 2. According to Zhang's work, it is as follows:[28]

$$0.5X + 399.5Y = 400 \cdot \mathrm{EF} \cdot X, \tag{5}$$

where X represents the intensity of fluorescence enhancement per micron in Ag-WL substrate, and Y represents the intensity of unenhanced per micron in sandwich structure. So the effective enhancement factor ($\mathrm{EF_{eff}}$) is X/Y. Based on formulas (4) and (5), the calculated EF and $\mathrm{EF_{eff}}$ values of the Ag-WL substrate are shown in Tables 1 and 2.

Table 1. The EF and $\mathrm{EF_{eff}}$ of the Ag-WL substrate were measured with 10^{-5} M RB aqueous solution.

Substrate	EF	$\mathrm{EF_{eff}}$
Ag-WL-15	1.21	165.2
Ag-WL-20	1.61	485.1
Ag-WL-25	1.64	513.9
Ag-WL-30	1.69	556.7
Ag-WL-35	1.91	731.3
Ag-WL-40	2.05	839.4
Ag-WL-45	1.70	558.4

Table 2. The EF and $\mathrm{EF_{eff}}$ of the Ag-WL substrate were measured with 10^{-5} M R6G aqueous solution.

Substrate	EF	$\mathrm{EF_{eff}}$
Ag-WL-15	1.43	348.0
Ag-WL-20	1.56	452.2
Ag-WL-25	1.84	671.7
Ag-WL-30	1.96	767.8
Ag-WL-35	2.08	868.9
Ag-WL-40	2.20	961.2
Ag-WL-45	1.68	543.3

The fluorescence intensity can be enhanced up to 839 times, showing that the Ag-WL substrate has excellent SEF effect.

3.4. The 3D-FDTD simulation

The 3D-FDTD is one of the methods to simulate the interaction between electromagnetic wave and complex system. Combining with the experimental results, the electromagnetic field enhancement of silver nanostructure substrate with the best performance of SEF effect is simulated theoretically to analyze the detail of hot spot distribution and electromagnetic filed enhancement.[29,30] Figure 6(a) is the constructed basic model diagram. A rectangular-shaped continuous wave incident into the nanostructure along the Z direction and the polarization direction is perpendicular to the Z direction, and the polarization direction of the laser was E direction, which is marked on Fig. 6(a). The calculated planes are P_1 and P_2, as shown in Fig. 6(b), and the calculated results are shown in Figs. 6(c) and 6(d). The electromagnetic enhancement distribution of the substrate can be clearly seen. P_1 and P_2 correspond to the X–Y plane and X–Z plane, respectively. In the P_1 plane, the hot spots are distributed in the gap of Ag nanoislands. The gap of lamellar structure at the bottom of wheat leaves brings many hot spots. In the P_2 plane, the semispherical protrusions on the substrate shows the distribution of hot spots not only on the top but also on the side, which is

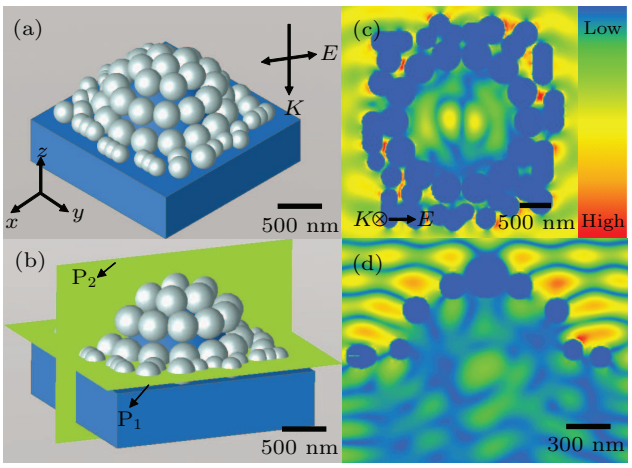


Fig. 6. (a) FDTD model of Ag-WL-40 substrate. (b) The calculated planes. (c) and (d) Spatial distribution of electric field intensities for the planes P_1 and P_2 in (b).

different from other SEF substrates. Various hot spots play an important role in generating both electromagnetic (EM) effect and enhanced fluorescence signals.

3.5. Reproducibility and stability of SEF substrate

Reproducibility and stability are also essential elements of an excellent SEF substrate. The reproducibility and stability of SEF substrate determines whether the substrate has practical application value, so it should be considered. Firstly, the reproducibility of the substrate was studied by using 10^{-5} M RB solution as the fluorescence reagent. We randomly selected 15 different positions from the Ag-WL-40 substrate, and the fluorescence spectrum measurement results are shown in Fig. 7(a). As can be seen, the position of the characteristic peak of RB aqueous solution does not shift, and the peak shape does not change. In addition, the reproducibility of Ag-WL-40 substrate was quantitatively evaluated by calculating the RSD, and the common expression of the relative standard deviation was given by the following equation:[31]

$$\mathrm{RSD} = \frac{\sqrt{\frac{\sum_{i=1}^{n}(I_I - \bar{I})^2}{n-1}}}{\bar{I}}, \tag{6}$$

where $\bar{I}$ is the average value of the measured fluorescence intensity, n is the number of experiments, and I_i is the fluorescence intensity measured in the i-th experiment. The fluorescence intensity distribution of the characteristic peak at 579 nm is drawn in Fig. 7(b). According to formula (6), the RSD at 579 nm is as low as 10.7%. The results show that the Ag-WL-40 substrate has good repeatability. Then, Fig. 7(c) shows the fluorescence spectra of 10^{-5} RB aqueous solution on Ag-WL-40 substrate for different time (0, 1, 2, 3, 4 weeks) under the same experimental conditions. It can be observed that the SEF performance of the substrate decreases gradually with the increase of the exposure time in the air. Figure 7(d) shows the variation of fluorescence intensity of RB aqueous solution at 579 nm with different exposure time of Ag-WL-40 substrate in air. When the Ag-WL-40 substrate was exposed to air for one week, the fluorescence intensity decreased by 8.8%, and when the Ag-WL-40 substrate was exposed to air for four weeks, the fluorescence intensity decreased by 28.2%. Therefore, with the increase of exposure time in air, the silver nanoislands deposited on the surface of wheat leaves were slightly oxidized, but there was still SEF effect, which indicated that the prepared Ag-WL-40 substrate showed excellent time stability.

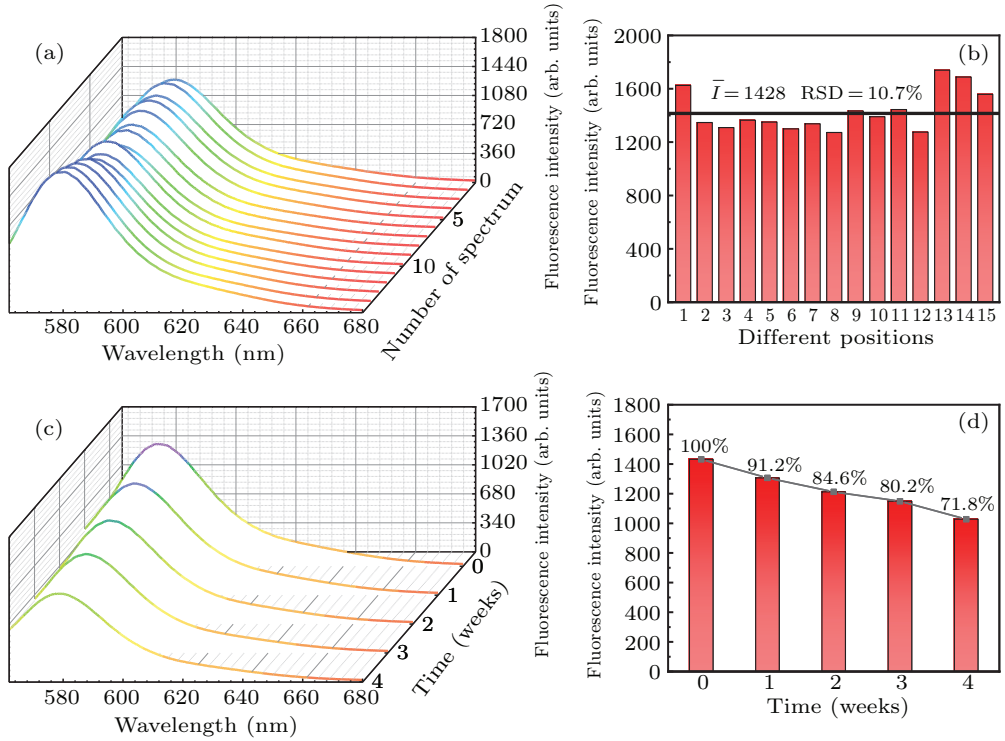


Fig. 7. (a) The fluorescence spectra of 10^{-5} M RB aqueous solution randomly were measured at different positions on Ag-WL-40 substrate. (b) The fluorescence intensities at 579 nm in (a). (c) Fluorescence spectra of 10^{-5} M RB aqueous solution at different detection time. (d) Fluorescence intensity change with the time of Ag-WL-40 substrate placed in air at 579 nm in (c).

3.6. Application of the Ag-WL-40 substrate

Research shows that CV is a toxic substance. It not only damages human body, but also has adverse effects on aquatic organisms and environment. Therefore, it is necessary to detect CV contents quickly and sensitively. Based on the fact that CV is also a series of triphenylmethane fluorescent dyes, the practical detection ability of SEF substrate was studied. According to the absorption spectrum in Fig. 5(b), we choose

580 nm as the excitation wavelength to detect the fluorescence spectrum of CV solution. Figure 8(a) shows the fluorescence spectra of different concentrations of CV solution on Ag-WL-40 substrate. The detection limit of CV is as low as 10^{-10} M. In addition, in order to quantitatively detect the concentration of CV, log$C$ and fluorescence intensity were fitted as shown in Fig. 8(b). The linear relationship of log C between 10^{-10} M and 10^{-4} M is $I = 356.3 \log C + 3668.9$, and the linear coefficient $R^2 = 0.992$. Meanwhile, the fluorescence intensity of Ag-WL-40 substrate was very stable even under NaCl concentration as high as 1000 mM, as shown in Fig. 8(c). It indicates that the substrate can be used to effectively detect the actual CV concentration.

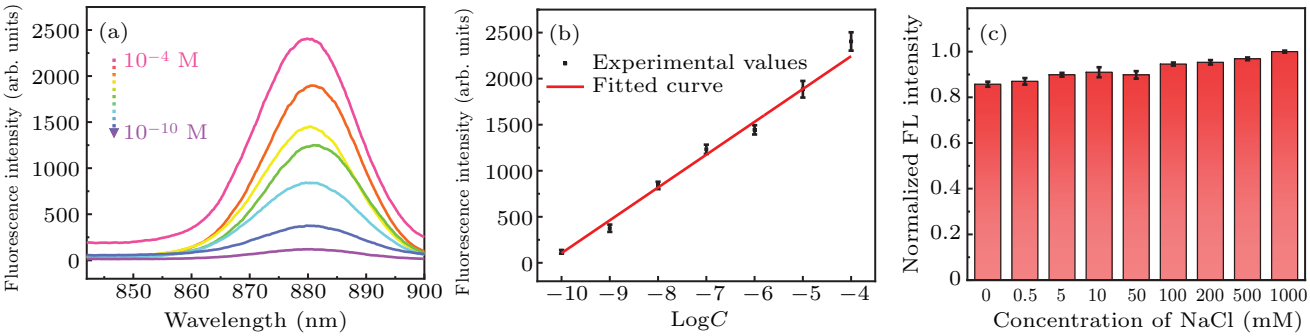


Fig. 8. (a) Fluorescence spectra of CV at different concentrations (10^{-10} M–10^{-4} M) on Ag-WL-40 substrate. (b) Linear calibration plot between the fluorescence intensity and CV concentration at 880 nm. (c) The fluorescence intensity of 10^{-5} M CV and NaCl solution in the Ag-WL-40 substrate at 880 nm.

4. Conclusion

In summary, a series of SEF substrates with excellent properties were prepared by depositing silver nanoislands on wheat leaves by magnetron sputtering system. The substrate with the best SEF effect, Ag-WL-40 substrate, was screened by RB solution, and the result was further verified repeatedly by R6G solution. Combined with the 3D-FDTD simulation method, it was found that the semi-spherical protrusions and the bottom lamellar structures of wheat leaves provided abundant hot spots. Finally, the quantitative detection of CV solution provides a simple, environmentally friendly and effective method for the detection of CV concentrations.

Acknowledgements

Project supported by the National Natural Science Foundation of China (Grant Nos. 21872119 and 22072127) and Science and Technology Project of Hebei Education Department, China (Grant No. ZD2019069).

References

[1] Huang Y, Zhang Y, Huo F, Wen Y and Yin C 2020 *Sci. China (Chem.)* **12** 1742
[2] Cheng Y, Wang J, Wei X, Guo D, Wu B, Yu L, Wang X and Shi Y 2015 *Chin. Phys. Lett.* **32** 117801
[3] Liu Y, Yi F, Badugu R, Lakowicz J R and Xu X 2012 *Chin. Phys. B* **21** 037803
[4] Wang K, Ma W, Xu Y, Liu X, Chen G, Yu M, Pan Q, Huang C, Li X, Mu Q, Sun Y and Yu Z 2020 *Chin. Chem. Lett.* **12** 3149
[5] Wang M, Shang Z, Yan X, Shi G, Cao H, Ma W and Jiao T 2021 *Opt. Commun.* **481** 126522
[6] Zhu X, Shi H, Zhang S, Chen Z, Zheng M, Wang Y, Xue S, Zhang J and Duan H 2019 *Acta Phys. Sin.* **68** 147304 (in Chinese)
[7] Wei D, Sudheendra L, Zhao J, Fu J and Goldys E M 2011 *Nanotechnology* **22** 325604
[8] Deng W, Drozdowicz-Tomsia K, Jin D and Goldys E M 2009 *Anal. Chem.* **81** 7248
[9] Gill R and LeRu E C 2011 *Phys. Chem. Chem. Phys.* **13** 16366
[10] Schmidtke C, Kloust H, Stús N B, Merkl J P, Tran H, Flessau S, Feld A, Schotten T and Weller H 2013 *Nanoscale* **5** 11783
[11] Sun J, Pi F, Ji J, Lei H, Gao Z, Zhang Y, Habimana J D, Li Z and Sun X 2018 *Anal. Chem.* **90** 3099
[12] Zhu X, Zhang S, Shi H, Chen Z, Quan J, Xue S, Zhang J and Duan H 2019 *Acta Phys. Sin.* **68** 247301 (in Chinese)
[13] Chang S, Eichmann S L, Huang T Y S, Yun W and Wang W 2017 *J. Phys. Chem. C* **121** 8070
[14] Xia Y, Gilroy K D, Peng H and Xia X 2017 *Angew. Chem. Int. Edit.* **56** 60
[15] Ma Y, Wu Z, Zhang L, Liu W and Zhang J 2015 *Chin. Phys. Lett.* **32** 94202
[16] Yin T, Jiang L and Shen Z 2018 *Chin. Phys. B* **27** 097803
[17] Omidvar A, RashidianVaziri M R, Jaleh B, Partovi Shabestari N and Noroozi M 2016 *Chin. Phys. B* **25** 118102
[18] Kinkhabwala A, Yu Z, Fan S, Avlasevich Y, Müllen K and Moerner W E 2010 *Nat. Photon.* **3** 654
[19] Guo L, Cao H, Cao L, Li N and Wang M 2021 *Opt. Express* **29** 5152
[20] Chen Y and Fang Y 2008 *Spectrochim. Acta A* **69** 733
[21] Meng F, Hu J, Wang H, Zou G, Cui J and Zhao Y 2019 *Acta Phys. Sin.* **68** 237801 (in Chubese)
[22] Shi G, Wang M, Zhu Y, Wang Y and Xu H 2018 *Appl. Surf. Sci.* **459** 802
[23] Nag A and Goswami D 2009 *J. Photoch. Photobio. A* **206** 188
[24] Lakowicz J R 2005 *Analytical Biochemistry* **337** 171
[25] Boyack R and Ru E 2009 *Phys. Chem. Chem. Phys.* **11** 7398
[26] Dong J, Zheng H, Yan X, Sun Y and Zhang Z 2012 *Appl. Phys. Lett.* **100** 051112
[27] Zhang Y, Dragan A and Geddes C D 2010 *J. Appl. Phys.* **107** 024302
[28] Ji Z, Xu S, Xu W, Bing Z and Ozaki Y 2010 *J. Raman Spectrosc.* **40** 31
[29] Wang X Y, Ma T T, Zhuang Y, Wang X D, Ning H Y, Shi H Y, Yu R L, Yan D, Huang H D and Bai Y F 2018 *Allergy* **73** 1232
[30] Yan X, Wang M, Sun X, Wang Y, Shi G, Ma W and Hou P 2019 *Appl. Surf. Sci.* **479** 879
[31] Shang Z, Wang M, Pan S, Sun X, Shi G, Yan X, Ma W and Jiao T 2019 *Opt. Commun.* **51** 345